



This open access document is published as a preprint in the Beilstein Archives with doi: 10.3762/bxiv.2019.69.v1 and is considered to be an early communication for feedback before peer review. Before citing this document, please check if a final, peer-reviewed version has been published in the Beilstein Journal of Organic Chemistry.

This document is not formatted, has not undergone copyediting or typesetting, and may contain errors, unsubstantiated scientific claims or preliminary data.

Preprint Title A toolbox of molecular photoswitches to modulate the CXCR3 chemokine receptor with light

Authors Xavier Gómez-Santacana, Sabrina M. de Munnik, Tamara A. M. Mocking, Niels J. Hauwert, Shanliang Sun, Prashanna Vijayachandran, Iwan J. P. de Esch, Henry F. Vischer, Maikel Wijtmans and Rob Leurs

Publication Date 15 Jul 2019

Article Type Full Research Paper

Supporting Information File 1 Gomez-Santacana Supporting Information.pdf; 2.7 MB

ORCID® iDs Tamara A. M. Mocking - <https://orcid.org/0000-0001-6490-4429>;
Niels J. Hauwert - <https://orcid.org/0000-0002-1217-1670>;
Prashanna Vijayachandran - <https://orcid.org/0000-0002-1047-538X>;
Henry F. Vischer - <https://orcid.org/0000-0002-0184-6337>; Maikel
Wijtmans - <https://orcid.org/0000-0001-8955-8016>; Rob Leurs -
<https://orcid.org/0000-0003-1354-2848>

License and Terms: This document is copyright 2019 the Author(s); licensee Beilstein-Institut.

This is an open access publication under the terms of the Creative Commons Attribution License (<http://creativecommons.org/licenses/by/4.0>). Please note that the reuse, redistribution and reproduction in particular requires that the author(s) and source are credited.

The license is subject to the Beilstein Archives terms and conditions: <https://www.beilstein-archives.org/xiv/terms>.

The definitive version of this work can be found at: doi: <https://doi.org/10.3762/bxiv.2019.69.v1>

A toolbox of molecular photoswitches to modulate the CXCR3 chemokine receptor with light

Xavier Gómez-Santacana[#], Sabrina M. de Munnik, Tamara A. M. Mocking, Niels J. Hauwert, Shanliang Sun, Prashanna Vijayachandran, Iwan J. P. de Esch, Henry F. Vischer, Maikel Wijtmans,* Rob Leurs*

Division of Medicinal Chemistry, Amsterdam Institute for Molecules Medicines and Systems (AIMMS) Vrije Universiteit Amsterdam, 1081 HZ, Amsterdam, The Netherlands.[#]Present address: Institute of Functional Genomics, Université de Montpellier, Unité 5302 CNRS and Unité U1191, INSERM, 34090 Montpellier, France.

* Corresponding author: m.wijtmans@vu.nl; r.leurs@vu.nl

Abstract

We report a detailed structure-activity relationship for the scaffold of VUF16216, a compound we have previously communicated as a small-molecule efficacy photoswitch for the peptidergic chemokine GPCR CXCR3. A total of 31 photoswitchable azobenzene ligands was prepared through various synthetic strategies and multistep syntheses. Photochemical and pharmacological properties were used to guide the design iterations. Investigations of positional and substituent effects reveal that halogen substituents on the *ortho* position of the outer ring are preferred for conferring partial agonism on the *cis* form of the ligands. This effect could be further expanded by an EDG group on the *para* position of the central ring. A variety of efficacy differences between the *trans* and *cis* forms emerges from these compounds. Tool compounds VUF15888 (**4d**) and VUF16620 (**6e**) represent more subtle efficacy switchers, while VUF16216 (**6f**) displays the largest efficacy switch, from antagonism to full agonism. The compound class disclosed here can aid in new photopharmacology studies of CXCR3 signaling.

Introduction

Photopharmacology is an emerging discipline at the boundaries of medicinal chemistry and photochemistry. Classical medicinal chemistry approaches make use of small-molecule ligands binding a target protein, thereby modifying its activity. Photopharmacological approaches use light-sensitive photochromic ligands that provide an advantageous and more precise pharmacological alternative, especially with respect to spatial and temporal precision.^{1,2} Photochromic ligands usually contain a molecular photoswitch (photoswitchable moiety) that under certain wavelengths of illumination undergoes an isomerization event, thereby changing the properties of the molecule and the binding affinity for the target protein³⁻⁵ or the intrinsic functional activity (efficacy).^{6,7} Despite the considerable number of photoswitches reported to date, such as spiropyrans, diarylethenes, fulgides or azobenzenes, the most vastly used moiety in the photopharmacology is the latter one. One of the main reasons is that an azobenzene has a relatively simple structure that can resemble various biaryl moieties of bioactive compounds: two aromatic rings linked with a bridge (e.g. amide, ether, alkane or alkyne).⁸ In the case of azobenzene the bridge is a diazene group (also called azo group) and depending on the wavelength of illumination, a linear *trans* isomer or a bent *cis* isomer can be obtained.⁹ In this way, if a biaryl moiety is replaced by an azobenzene (i.e. azologization approach), there is relatively good chance that one of the resulting photoisomers will have a similar spatial disposition to the original biaryl unit and, therefore, a similar biological activity that might change upon isomerization of the

azobenzene.⁸ The second reason for the success of azobenzene in the photopharmacology field is the robust photoisomerization. It provides typically high yields of photoisomerization with relatively low intensity of light and minimal photobleaching even over hundreds of cycles. A third reason is the relatively high synthetic accessibility to azobenzenes. All these properties make azobenzene compounds ideal molecular photoswitches to control protein activity and physiological events with light.

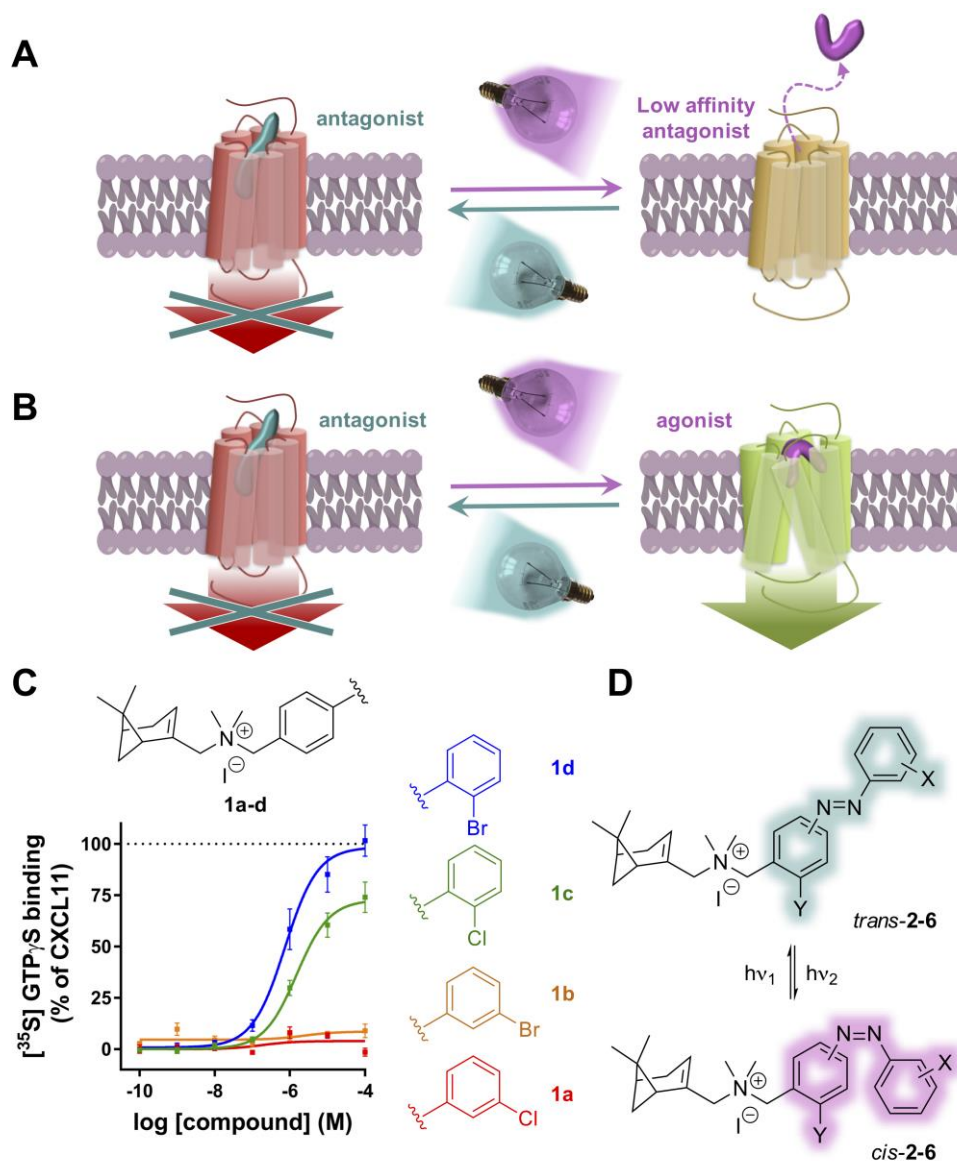


Figure 1: Design of the CXCR3 efficacy photowitchable ligands. A,B) Schematic representation of a GPCR photochromic ligand that photoisomerises and thereby photoswitches (A) binding affinity and/or (B) functional efficacy. C) General structure and exemplary functional dose-response curves of the parent biaryl family of CXCR3 ligands disclosed in Wijtman *et al.*¹⁷, in which *ortho* substitution on the outer aromatic ring gives partial or full agonists, while *meta* substitution provides antagonists. D) Azologization of the biaryl moiety provides a family of photowitchable CXCR3 small-molecule ligands.

A number of protein targets have now been explored with photochromic small-molecule ligands, such as ion channels, microtubules, enzymes and G protein-coupled receptors (GPCRs)^{1,10}. We focus our photopharmacology research on GPCRs,^{3,7,11} which constitutes a superfamily of membrane proteins

that regulate many physiological processes.¹² Despite the high relevance of GPCRs both functionally and as a drug target¹², the first synthetic GPCR photochromic small-molecule ligands appeared only five years ago¹³⁻¹⁵. Since then a range of GPCRs has been targeted in photopharmacology¹⁰. Most of them belong to the three rhodopsin-, secretin- and glutamate-like subfamilies and involve GPCRs that endogenously bind small-molecule ligands. The ensuing photochromic GPCR ligands are usually orthosteric and the photoswitching generally affects the functional potency^{4,11,16} and/or the affinity binding^{3-5,11} of the ligand (Figure 1A). However, GPCRs that endogenously bind very large molecules (large peptides or proteins) can be also targeted by allosteric photochromic ligands. Indeed, in an initial communication⁷, we recently reported a photochromic ligand class that activates the chemokine CXCR3 receptor (CXCR3), a GPCR endogenously activated by peptides CXCL9, CXCL10 and CXCL10 and involved in inflammatory responses. In fact, the new photochromic ligand for CXCR3 represents the first photochromic small-molecule ligand class that harbors a dynamic efficacy photoswitch (from antagonism to agonism) on a peptidergic GPCR (Figure 1B). Here, we will present the rationale and synthetic strategies behind this series of compounds, a detailed analysis of the molecular determinants that control the efficacy of the ligands (Structure-Activity Relationship) and a toolbox of pharmacologically useful photoswitchable small-molecule CXCR3 agonists.

Results and discussion

Azologization design

Chemokine receptor CXCR3 can be activated by the chemotactic peptides CXCL11, CXCL10 and CXCL9, but also synthetic small-molecule ligands can bind to CXCR3.¹⁸ Multiple small-molecule CXCR3 antagonist scaffolds have been disclosed but small-molecule CXCR3 agonists are scarce and are mostly limited to peptidomimetics¹⁸. Our published biaryl series represents a notable exception to the latter.¹⁷ The general scaffold of these ligands consists of a polycycloaliphatic anchor and a biaryl moiety both linked to an ammonium ion. Depending on the substitution pattern of this biaryl moiety, a broad spectrum of efficacies for CXCR3 can be obtained, i.e. from antagonists to partial agonists and full agonists (Figure 1C).¹⁷ *Meta* and *para* substitution yields antagonists (exemplified by **1a-b**), while *ortho* substitution with halogen atoms provides agonists, exemplified by partial agonist **1c** and equal full agonists **1d** and **1e** (VUF11418, Figure 2A). A tentative explanation for this efficacy switch included a variation of the dihedral angle of the biaryl moiety, an increase of the electron density in the biaryl unit and/or a postulated halogen bond of the halogen substituent to the binding site of the receptor.¹⁷

In order to obtain an efficacy photoswitching, we opted for replacing the biaryl moiety for an azobenzene in an azologization approach (Figure 1D) with the expectation that the isomerization of the azobenzene would provide changes in 3D shape that are similar to those observed in the biaryl series. To reinforce this hypothesis, molecular alignments were performed with MOE¹⁹ in which **1e** was used as a model for full agonism (Figure 2). Its 3D structure was superposed with both the *trans* and *cis* isomers of parent azobenzene compound **2a** allowing flexibility of the molecules except for the conformation of the *trans* and *cis* azobenzene moieties, which were fixed in the lowest energy conformation to ensure a shape that has also been validated by crystallographic data.²⁰ The results show a reasonable overall alignment between *trans*-**2a** and the agonist **1e** (Figure 2B), since the planar azobenzene is partially overlapping with the biaryl moiety. However, the two aromatic rings of both compounds can evidently not be in exactly the same plane because the azobenzene moiety is planar while the tilting of the dihedral angle of the biaryl moiety of **1e** was speculated to be associated with

its agonist activity (*vide supra*).¹⁷ The alignment of the *cis* isomer of **2a** with agonist **1e** is very different. The outer aromatic ring of *cis*-**2a** goes out of plane and is now occupying the space that is also occupied by the iodine atom of **1e**. These calculations indicate that CXCR3 agonism is more likely to be associated with the *cis* isomer than with the *trans* isomer in our designed azobenzenes.

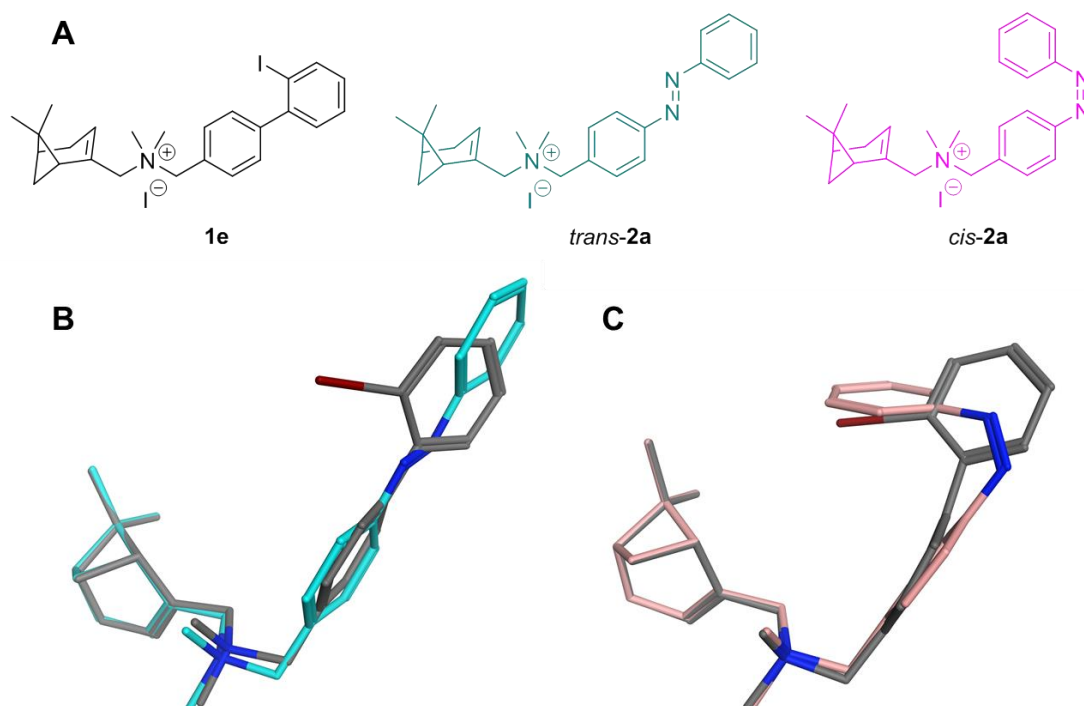
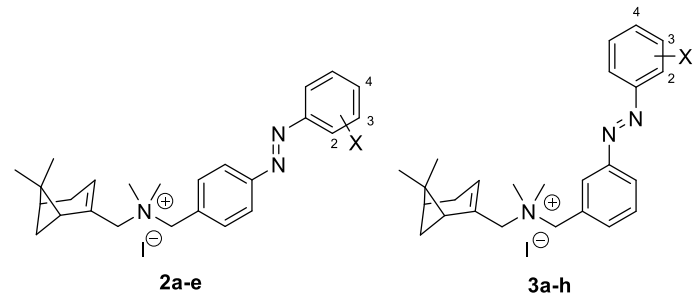


Figure 2: Conformational alignment of a biaryl CXCR3 agonist with a designed azobenzene analogue. A) 2D structure of biaryl CXCR3 agonist **1e** and designed ligand *trans*-**2a** and *cis*-**2a**. B-C) Alignments of **1e** (grey carbon atoms) and **2a**, in which the *trans* and *cis* isomers are shown in (B) turquoise and (C) light magenta carbon atoms, respectively. The iodine atom is shown in red for clarity.

Synthesis of azobenzene analogues and exploration of substitution pattern on the outer aromatic ring

In addition to unsubstituted azobenzene analogue **2a**, we explored the substitution pattern of the outer aromatic ring with chlorine atoms in the *ortho*, *meta* and *para* position (compounds **2b-d** respectively) to also assess the possibility of agonism provided by a halogen bond. Compound **2e**, which contains a bromine atom in the *ortho* position, was also tested since this atom type provides full agonist activity of parent **1d**. The synthesis of the compounds **2a-e** was performed according to the strategies depicted in Scheme 1. The intermediate **7** was prepared as described previously by us²¹ and was used in a reductive amination with 4-nitrobenzaldehyde (**8a**) to give the corresponding tertiary amine **9a** in high yield. The nitro group of **9a** was subsequently reduced by SnCl₂ in high yield. The resulting aniline **10a** was used to obtain the azocompounds **12a-e** in varying yields through a Mills reaction with the corresponding nitroso compound **11a-e**, which were commercially available or prepared as described in our previous communication.⁷ A final methylation of the tertiary amine **12a-e** with MeI in DCM and subsequent precipitation with MTBE gave **2a-e** as orange powders with ≥99% *trans* isomer in moderate to high yield.

Table 1: Structures and results of photochemical, binding and functional characterization of compounds 2a-e and 3a-h



| Cmpd | Photochemistry | | | | | CXCR3 binding affinity | | | | | Functional CXCR3 activity | | | | |
|-----------|----------------|---|---|--|-----|-------------------------------------|---|---------------|------------------|-----|------------------------------------|-----|--|-----|-------------------------|
| | X | λ_{\max} <i>trans</i> π - π^* | λ_{\max} <i>cis</i> n - π^* | PSS ₃₆₀ (area % <i>cis</i>) ^a | SEM | pK_i <i>trans</i> ^b | pK_i SEM PSS ₃₆₀ ^b | pK_i SEM | PAS ^c | | E (%) <i>trans</i> ^d | SEM | E (%) PSS ₃₆₀ ^e | SEM | PDE (%) ^f |
| 2a | H | 321 | 422 | 88.3 | 0.8 | 6.3 | 0.0 | 5.7 | 0.1 | 4.0 | -11.0 | 2.3 | -8.3 | 0.7 | 2.7 |
| 2b | 2-Cl | 323 | 416 | 84.9 | 0.5 | 6.3 | 0.0 | 5.8 | 0.1 | 3.2 | 2.4 | 4.3 | 11.1 | 2.0 | 8.7 |
| 2c | 3-Cl | 320 | 421 | 79.2 | 0.9 | 6.5 | 0.0 | 6.3 | 0.0 | 1.6 | -10.3 | 3.5 | -9.6 | 2.7 | 0.7 |
| 2d | 4-Cl | 330 | 423 | 89.7 | 0.5 | 6.6 | 0.0 | 6.0 | 0.0 | 4.0 | -9.8 | 3.5 | -2.7 | 3.6 | 7.1 |
| 2e | 2-Br | 324 | 421 | 87.2 | 0.5 | 6.4 | 0.0 | 5.9 | 0.1 | 3.2 | 7.0 | 1.6 | 22.7 | 1.5 | 15.7 |
| 3a | H | 320 | 423 | 82.0 | 1.5 | 6.0 | 0.1 | 5.4 | 0.1 | 4.0 | -11.6 | 2.2 | -4.7 | 1.7 | 6.9 |
| 3b | 2-Cl | 323 | 419 | 85.0 | 0.5 | 6.3 | 0.0 | 5.6 | 0.0 | 5.0 | -4.7 | 1.7 | 17.4 | 3.7 | 22.1 |
| 3c | 3-Cl | 317 | 421 | 83.4 | 0.4 | 6.3 | 0.0 | 5.8 | 0.0 | 3.2 | -8.4 | 2.2 | -0.4 | 1.6 | 8.0 |
| 3d | 4-Cl | 325 | 424 | 92.0 | 0.3 | 6.4 | 0.0 | 5.7 | 0.0 | 5.0 | -8.1 | 2.6 | 1.7 | 2.3 | 9.8 |
| 3e | 2-Br | 323 | 421 | 88.9 | 0.4 | 6.3 | 0.0 | 5.7 | 0.1 | 4.0 | -5.8 | 1.7 | 25.1 | 2.0 | 30.9 |
| 3f | 2-I | 323 | 422 | 80.9 | 0.2 | 6.2 | 0.0 | 5.8 | 0.1 | 2.5 | -4.0 | 1.2 | 15.8 | 1.3 | 19.8 |
| 3g | 3-I | 318 | 422 | 82.5 | 1.5 | 6.1 | 0.1 | 6.1 | 0.0 | 1.0 | -11.1 | 0.6 | -7.6 | 2.3 | 3.5 |
| 3h | 4-I | 337 | 422 | 91.1 | 1.1 | 6.0 | 0.0 | 5.7 | 0.0 | 2.0 | -15.3 | 1.1 | 5.4 | 1.5 | 20.7 |

^a % of *cis* isomer at the photostationary state (PSS₃₆₀) in PBS (25 μ M) measured after being pre-irradiated at 360 nm as obtained by LC/MS integration of the *cis* and *trans* isomer signals at 265 nm. The mean and SEM of at least two experiments are shown.

^b Binding affinity of *trans* isomer or PSS₃₆₀ as measured using [³H]-VUF11211 displacement. The mean and SEM of at least three experiments are shown.

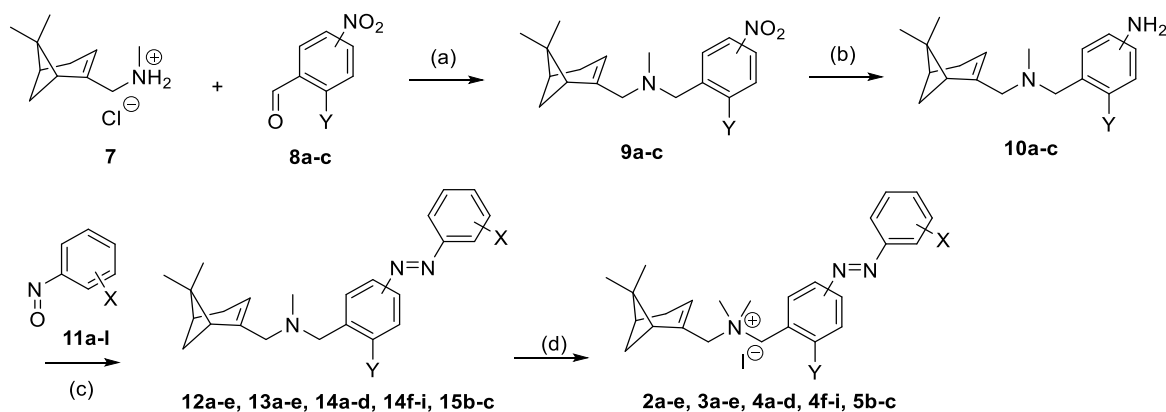
^c The photoinduced affinity shift (PAS) was calculated as the ratio of the K_i *trans* and K_i PSS₃₆₀.

^d Normalized CXCR3 functional activity of *trans* isomer (10 μ M) in the dark (efficacy of **1d** set at 100% activity). The mean and SEM of at least three experiments are shown.

^e Normalized CXCR3 functional activity of a sample (10 μ M) pre-irradiated at 360 nm to reach the photostationary state in the dark (efficacy of **1d** set at 100% activity). The mean and SEM of at least three experiments are shown.

^f The photoinduced difference of efficacy (PDE) was obtained by subtracting E *trans* from E PSS₃₆₀.

Next, we characterized the photochemical properties of **2a-e**, including absorption maxima, wavelengths of illumination and percentage of conversion from *trans* to *cis* in the photostationary state (PSS). First, UV-Vis absorption spectra were measured in the dark and after illumination with wavelengths of 360 nm, 434 nm or 490 nm. In all cases the spectrum measured in the dark showed a large band between 320 and 330 nm that corresponds to the π - π^* transition of the *trans* isomer (Figure S1A). After irradiating with different wavelengths, the proportion of *trans* and *cis* isomer varies to reach a photostationary state (PPS). For example, after irradiating with 360 nm the π - π^* transition band of the *trans* isomer can barely be observed, but a less intense wide band around 420 nm appears, which corresponds to the n - π^* transition of the *cis* isomer (Figure S1A). This indicates that a PPS of high percentage of *cis* isomer has been reached. In fact, due to the bistable nature of both photoswitch used, the percentage of each photoisomer can be quantified by analytical chromatography (LC-MS). For **2a-e** after illumination at 360 nm, PPS values of 79-90% of *cis* isomer were obtained. After re-illuminating these samples at 434 nm, the π - π^* transition band of the *trans* isomer re-appears, indicating a high percentage of *trans* isomer at that PSS.



Scheme 1: Synthetic strategies for compounds 2a-e, 3a-e, 4a-d, 4f-i and 5b-c. Reagents and conditions: (a) i) TEA (1.1-1.6 eq), DCM, rt, 10-30 min; ii) NaBH(OAc)₃ (1.6 eq), rt, 6-16 h, 91-97%; (b) SnCl₂ (5.0 eq), EtOH, 75 °C, 2h, 87%-quant; (c) AcOH/DCM, rt, 1-5 d, 23-73%, (d) MeI (20 eq), DCM, rt, 6-72 h, 41-97%.

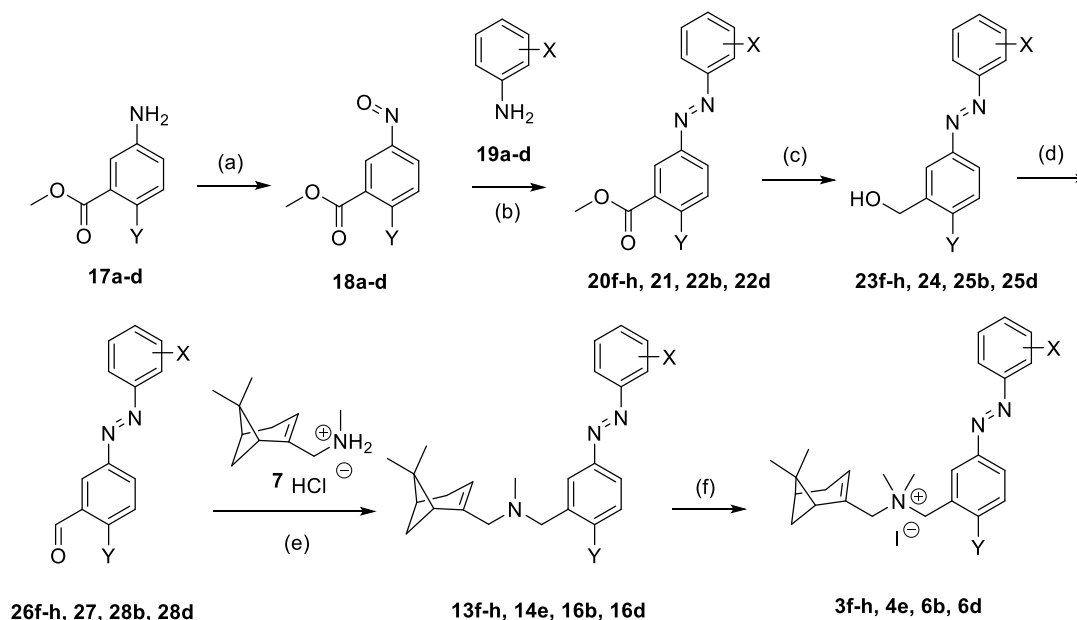
Next, the CXCR3 binding properties of **2a-e** were measured (Table 1) in a competition binding assay versus displacement of a radiolabeled small-molecule CXCR3 antagonist ([³H]-VUF11211²²). These experiments were performed with samples under dark conditions to ensure the $\geq 99\%$ *trans* isomer and with samples previously illuminated with 360-nm light to obtain a high percentage of *cis* compound in the PSS₃₆₀. Compounds **2a-e** under dark conditions (*trans* isomers) bind CXCR3 with K_i values in the high nanomolar range. In contrast, compounds **2a-e** after 360 nm illumination bind CXCR3 with K_i values in the low micromolar range, although the observed photoinduced affinity shifts (PAS) are not large (< 4.0-fold). To assess if the compounds have agonist or antagonist activity on CXCR3-mediated signaling, a functional [³⁵S]-GTP γ S accumulation assay was performed with the compounds **2a-e** at 10 μ M (Table 1). In this assay, we observed that most of the compounds are not activating the CXCR3 receptor in either *cis* or *trans* configuration, which indicates that the compounds bind to the receptor as antagonists. However, *cis*-**2b** and, more notably, *cis*-**2e** show a small partial agonist activity (11% and 23% respectively) that gives a hint of a slight photoswitching of their efficacy. Both compounds have a halogen atom on the *ortho* position of the outer ring, which seems to reaffirm the importance of the *ortho* halogen atoms effect observed in the biaryl series.¹⁷ However, the difference in efficacy between *cis* and *trans* isomers (defined as PDE) needed to be improved.

Optimization of positioning of azobenzene unit

Aiming to improve the position and direction of the halogen atom, we next designed a subseries with the azo group at the *meta* position of the central ring (scaffold **3**) instead of at the *para* position as in **2a-e**. The analogue without halogen substitution (**3a**) as well as Cl/Br analogues comparable to the first series (**3b-e**) were prepared. Moreover, since the importance of the presence of a halogen in the outer ring was suggested in **2**, compounds **3f-h**, which include an iodine atom on the *ortho*, *meta* and *para* positions respectively, were synthesized.

The synthesis of compounds **3a-e** was performed following the strategies shown in Scheme 1 as disclosed for compounds **2a-e**. Briefly, a reductive amination of **7** and **8b** gave nitro compound **9b**, which after reduction to **10b**, coupling with nitroso compound **11a-e** to **13a-e** and methylation gave iodide salts **3a-e** with purities of *trans* isomers $\geq 99\%$ and overall yields similar to the ones obtained for **2a-e**. However, 2-iodonitrosobenzene cannot be accessed through oxidation of the corresponding aniline owing to oxidation sensitivity of the iodine atom. Therefore, an alternative route had to be used to synthesize **3f-h** (Scheme 2). The route begins with the oxidation of methyl 3-aminobenzoate (**17a**)

using Oxone[®] to obtain a crude nitroso-product **18a**, which was used in a Mills reaction with an iodoaniline (**19a-c**) at 100 °C to obtain azobenzenes **20g-h** in high yields and *ortho*-analogue **20f** in a decreased yield presumably due to steric hindrance. The methyl ester was selectively reduced with DIBAL-H to benzyl alcohols **23f-h**, which were oxidized with Dess Martin periodinane to the corresponding benzaldehyde **26f-h**. Reductive amination of **26f-h** with **7** gave the tertiary amine **13f-h**. Methylation with iodomethane and subsequent precipitation gave **3f-h** as orange powders with $\geq 99\%$ *trans* isomer in high yields.



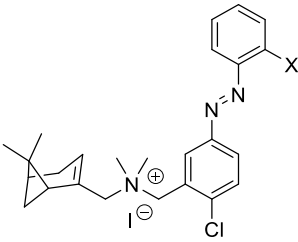
Scheme 2: Synthetic strategies for compounds 3f-h, 4e, 6b, and 6d. Reagents and conditions: (a) Oxone[®] (2.0 eq), DCM/H₂O 1:4, rt, 2 h, 91-98%; (b) AcOH, 100°C, 16-20 h, 61-96%; (c) i) DIBAL-H (3.0-4.0 eq), THF, 0-5 °C to rt, 2-4 h; ii) NH₄Cl (aq), Rochelle salt (10% aq), EtOAc, 1-2 h, 76-99%; or for **23h** i) DIBAL-H (1.2 eq), DCM, -78 °C, 1h; ii) MeOH, -78 °C to rt, 0.5 h, iii) Rochelle salt (10% aq), 3 h, 45%; (d) Dess Martin periodinane (1.0 eq), DCM, rt, 1-2 h, 68-97%; (e) i) TEA (1.1-1.6 eq), DCM, rt, 10-30 min; ii) NaBH(OAc)₃ (1.6 eq), rt, 6-16 h, 69-96%; (f) MeI (20 eq), DCM, rt, 6-72 h, 79-95%.

The photochemical properties of **3a-h** were very similar to those of **2a-e**. For the *trans* isomers, the maximum of the $\pi\text{-}\pi^*$ band is located around 318-325 nm, with the exception of **3h** which has an iodine atom on the *para* position and arguably confers a larger electron delocalization of π electrons that is translated to a shifting of the band to lower energy wavelength (337 nm). PSS values of 81-92% were obtained when illuminating with 360 nm light. The binding properties of **3a-h** also result in outcomes similar to those of **2a-e**. That is, K_i values were in the high nanomolar range for the *trans* isomers with no or low PAS values (1.0-5.0-fold) after isomerization. In single-dose functional assays, all *trans* isomers do not substantially activate CXCR3, whereas three of the *cis* isomers could weakly to substantially activate CXCR3 (**3b**: 17%, **3e**: 25% and **3f**: 16%). Interestingly, these three compounds are the only ones to include a halogen atom on the *ortho* position of the outer azobenzene ring, as is the case with *para* compounds **2b** (11%) and **2e** (23%). However, compared to the latter, *meta* compounds **3b,e,f** display an agonist effect that is slightly higher. Increasing the size of the *ortho*-halogen does not guarantee a maximal agonist effect, as the absolute activity of **3f** is lower than that of its Br analogue **3e**. Nevertheless, evidence emerged that the *ortho*-position of the outer aromatic ring in scaffold **3** is important to achieve agonist activity of the *cis* isomer, but it should be complemented with other strategies to further increase intrinsic activity.

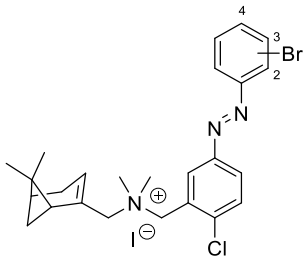
Substituent effects on the outer ring

One of the postulated contributors to the CXCR3 agonism effect of parent biaryls such as **1d** and **1e** is the increased π electron density of the aromatic rings.¹⁷ A way to translate this effect to the azobenzene system is by including a π -donating substituent on the aromatic system. For synthetic access and thus rapid exploration, we chose a Cl atom as mildly π -EDG group (even though it is σ -EWG) on the *para* position of the inner ring with respect to the azo bond (i.e. the *ortho* position with respect to the benzylic position) to afford subseries **4**. This π -electron delocalization, besides increasing the electron density of the azobenzene unit, may also improve the *trans-cis* azobenzene isomerization and give the possibility to obtain a PSS of more than 90% *cis*. In terms of the outer ring, and given that *ortho* halogen atoms in subseries **2-3** play an important role in conferring the *cis* isomer with partial agonism, in subseries **4** we explored halogen atoms and groups differing in e.g. steric and electronic properties (Me, CF₃, OMe, OCF₃). The electron donating groups in this series (Me and OMe) also increase the electron density of the azobenzene system, which in turn helps in probing a possible electron density contributor to agonism (*vide supra*).

Table 2: Structure and results of photochemical, binding and functional characterization of compounds 4a-i and 5b-c



4a-i



4d, 5b-c

| Cmpd | Photochemistry | | | | | CXCR3 binding affinity | | | | | Functional CXCR3 activity | | | | |
|-----------|--------------------|----------------------------------|--------------------------------|--|-----|--|-----|--|-----|------------------|---------------------------|-----|---------------------------------|-----|------------------|
| | X | λ_{\max} <i>trans</i> | λ_{\max} <i>cis</i> | PSS ₃₆₀ (area % <i>cis</i>) ^a | SEM | pK _i <i>trans</i> ^b | SEM | pK _i PSS ₃₆₀ ^b | SEM | PAS ^c | E (%) | | PDE | | |
| | | π - π * | n- π * | <i>cis</i> | | | | | | | <i>trans</i> ^d | SEM | PSS ₃₆₀ ^e | SEM | (%) ^f |
| 4a | H | 326 | 424 | 91.8 | 1.2 | 5.8 | 0.0 | 5.2 | 0.0 | 4.0 | -2.9 | 1.0 | 12.1 | 0.7 | 15.0 |
| 4b | 2-F | 330 | 420 | 93.0 | 0.2 | 5.6 | 0.0 | 5.0 | 0.0 | 4.0 | -4.9 | 0.5 | 14.6 | 0.8 | 19.5 |
| 4c | 2-Cl | 330 | 419 | 92.8 | 0.1 | 5.8 | 0.0 | 5.3 | 0.1 | 3.2 | 2.3 | 1.6 | 36.9 | 2.0 | 34.6 |
| 4d | 2-Br | 328 | 422 | 92.6 | 0.2 | 5.9 | 0.0 | 5.6 | 0.0 | 2.0 | 13.6 | 2.4 | 49.6 | 2.6 | 36.0 |
| 4e | 2-I | 330 | 424 | 79.9 | 1.2 | 5.7 | 0.0 | 5.7 | 0.0 | 1.0 | 16.0 | 1.4 | 37.1 | 0.5 | 21.1 |
| 4f | 2-Me | 332 | 428 | 94.9 | 0.1 | 5.9 | 0.0 | 5.3 | 0.0 | 4.0 | 6.9 | 3.1 | 32.2 | 1.1 | 25.3 |
| 4g | 2-CF ₃ | 326 | 424 | 58.0 | 1.1 | 5.9 | 0.0 | 5.7 | 0.0 | 1.6 | 10.5 | 1.6 | 8.3 | 1.5 | -2.2 |
| 4h | 2-OMe | 328 | 427 | 92.6 | 0.2 | 5.4 | 0.0 | 5.0 | 0.0 | 2.5 | 4.9 | 1.2 | 18.7 | 1.1 | 13.8 |
| 4i | 2-OCF ₃ | 326 | 422 | 78.8 | 1.2 | 5.9 | 0.0 | 5.6 | 0.0 | 2.0 | -3.0 | 2.0 | -2.4 | 3.1 | 0.6 |
| 4d | 2-Br | 328 | 422 | 92.6 | 0.2 | 5.9 | 0.0 | 5.6 | 0.0 | 2.0 | 13.6 | 2.4 | 49.6 | 2.6 | 36.0 |
| 5b | 3-Br | 324 | 420 | 87.4 | 1.2 | 5.7 | 0.1 | 5.6 | 0.0 | 1.3 | -1.7 | 1.9 | 10.5 | 0.5 | 12.2 |
| 5c | 4-Br | 335 | 427 | 93.8 | 0.5 | 6.2 | 0.0 | 5.6 | 0.0 | 4.0 | -7.2 | 1.8 | 1.8 | 2.5 | 9.0 |

^a % of *cis* isomer at the photostationary state (PSS₃₆₀) measured after being pre-irradiated at 360 nm as obtained by LC/MS integration of the *cis* and *trans* isomer signals at 265 nm. The mean and SEM of at least two experiments are shown.

^b Binding affinity of *trans* isomer or PSS₃₆₀ in PBS (25 μ M) as measured using [³H]-VUF11211 displacement. The mean and SEM of at least three experiments are shown.

^c The photoinduced affinity shift (PAS) was calculated as the ratio of the K_i *trans* and K_i PSS₃₆₀.

^d Normalized CXCR3 functional activity of *trans* isomer 10 μ M in the dark (efficacy of **1d** set at 100% activity). The mean and SEM of at least three experiments are shown.

^e Normalized CXCR3 functional activity of a sample 10 μ M pre-irradiated at 360 nm to reach the photostationary state in the dark 10 μ M (efficacy of **1d** set at 100% activity). The mean and SEM of at least three experiments are shown.

^f The photoinduced difference of efficacy (PDE) was obtained by subtracting E *trans* from E PSS₃₆₀.

The synthesis of **4a-d** and **4f-i** was performed following the route shown in Scheme 1. Briefly, **7** was used in a reductive amination with 2-chloro-3-nitrobenzaldehyde (**8c**) to give nitrocompound **9c** which was reduced to aniline **10c** and used to obtain the azo compounds **14a-d,f-i** in variable yields through a Mills reaction with the corresponding nitroso compound **11a-b,e-j**. Methylation of **14a-d,f-i** with MeI yielded compounds **4a-d,f-g,i** as orange powders with $\geq 99\%$ *trans* isomer in moderate to high yields. Salt **4h** did not precipitate after treatment with TBME and was isolated as an oil which retained substantial amounts of MTBE solvate even after extensive drying. For **4e**, we used the strategy as explained for iodocompounds **3f-h** (*vide supra*). Briefly, the route (Scheme 2) consists of the oxidation of methyl 5-amino-2-chlorobenzoate (**17c**) with Oxone[®] to **18c**, which was used in a Mills reaction with an 2-iodoaniline (**19a**) to yield azobenzene **21**. The methyl ester was selectively reduced with DIBAL-H and the resulting alcohol **24** oxidized with Dess Martin periodinane to benzaldehyde **27**. Reductive amination of **27** with **7** to **14e** and subsequent methylation gave **4e** as an orange powder with $\geq 99\%$ *trans* isomer.

Photochemical characterization of **4a-i** (Table 2) gives similar results as observed for subseries **2-3**, with *trans* π - π^* bands having a maximum between 326 and 332 nm and PSS values generally amounting to over 90% of *cis* isomer after illuminating with 360-nm light, as predicted as a result of the electron localization provided by the chlorine atom in the central aromatic ring. Compounds **4e**, **4i** and most notably **4g** deviate from this trend, since the percentage of *cis* isomer in the PSS is significantly lower (58-80%).

Trans-4a-i show a slight decrease in binding affinity compared to the subseries **2** and **3**, amounting to low micromolar values (Table 2). Moreover, PSS affinity values are also modest, with only four compounds that have a PAS > 2.5 (**4a-c,f**). However, functional data from [³⁵S]-GTP γ S assays provided encouraging results. While all *trans* isomers of **4a-i** do not or only weakly activate the receptor, some of the *cis* isomers clearly behave as partial agonists. The highest efficacy is exerted by *cis-4c-f* with E values between 30-50% at 10 μ M. Interestingly, one of these compounds (**4f**) includes a methyl group as *ortho* substituent on the outer ring and its agonist effect at PSS amounts to 32%, possibly questioning one of our hypotheses that a halogen bond is involved in inducing CXCR3 agonism.

Similar to subseries **3**, the substituent on the *ortho* position of the outer aromatic ring appears to be a driver for the agonist activity of the corresponding *cis* isomer. Starting from weak partial agonist **4a** (X=H), the agonist response of the *cis* increases with increasing halogen atom (**4b-d**) to a maximal response with **4d** (X=Br) having an agonist effect of 50%. However, when X = I (**4e**) the agonist activity is reduced, as also observed in the **3** subseries (compare **3d** to **3e**). In general, the agonist effects and PDE values exerted by subseries **4** are larger than those exerted by **3** (Figure 3). This could be explained by the effect of the Cl atom present in the **4** subseries, that may confer a rise in electron density to the azobenzene necessary to increase the efficacy of the *cis* ligand.

In both subseries **3** and **4**, a bromine atom on the *ortho* position of the outer ring gives optimal results in providing CXCR3 efficacy photoswitching (Figure 3). To confirm this for subseries **4**, the analogues of **4d** with the bromine on the *meta* and *para* position (**5b** and **5c**, respectively) were also synthesized. The synthetic route (Scheme 1) utilized **10c** and synthesized 3- and 4-bromonitrosobenzene (**11k,l**) to form azobenzenes **15b,c**, which were methylated to obtain **5b-c**. The binding affinities (Table 2) obtained for the *trans* and *cis* isomers were all in the micromolar range. More importantly, when comparing functional results of **4d**, **5b** and **5d**, the preference for a Br atom on the *ortho*-position can

also be reaffirmed for subseries **4**, because *cis*-**5c** is an antagonist, while *cis*-**5b** shows only a weak activity (Table 2).

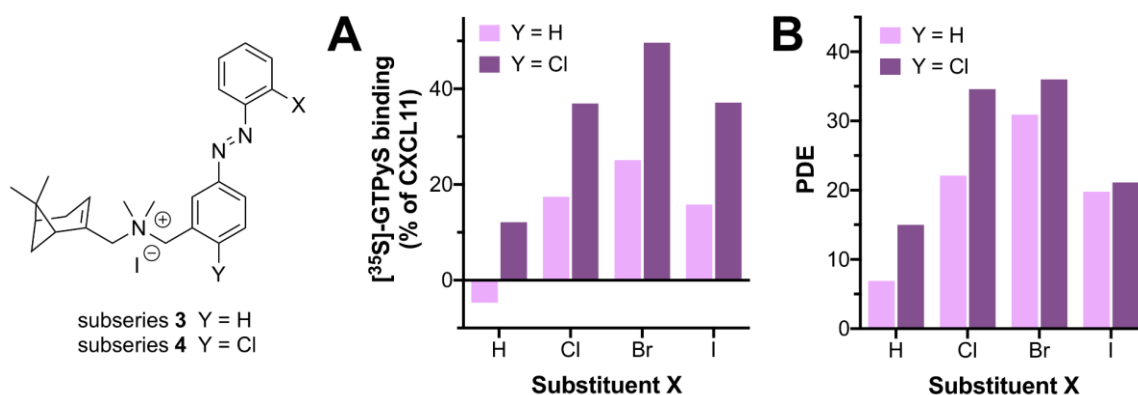


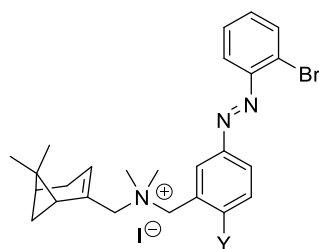
Figure 3: Comparison of compounds belonging to the subseries 3 or 4 with a halogen substitution on the *ortho* position of the outer ring (X). (A) Activities of *cis* isomers at 10 μM on CXCR3-mediated G protein activation. (B) PDE values at 10 μM .

Substituent effects on the central ring

As shown, substitution of the outer ring with an *ortho* bromine in conjunction with a Cl substituent on the central ring appeared to pave the way for efficacy photoswitching but there was still room for improvement. Our strategy in this final optimization round was to replace the mildly π -EDG Cl atom with other groups. Thus, to aim for a full-agonist *cis* compound, the sub-series **6** was synthesized. In this subseries, different groups at the *para* substitution of the central ring (Y) in combination with the *ortho* Br atom in the outer aromatic ring was used to explore optimal electron densities in the azobenzene system. Besides the H and Cl already explored (**3b** and **4d**, respectively), other groups including an EWG halogen atom (F, **6b**), EDG halogen atoms (Br, **6d** and I, **6e**) and stronger EDG moieties such as OMe (**6f**), *OiPr* (**6f**), SMe (**6f**) and NMe₂ (**6f**) were introduced.

Compounds **6b** and **6d** were synthesized by the route shown in Scheme 2, using in this case halogenated methyl aminobenzoates **17b-c** and 2-bromo-aniline **19d**. The synthetic route for compound **6e** proved more challenging. The route of Scheme 1 could not be readily used because the corresponding iodinated nitroprecursor **8** is not commercially available, nor could the second route (Scheme 2) since the iodine would likely be sensitive to the first oxidation step. Therefore, we designed a new route (Scheme 3). The starting point was the advanced intermediate **28b** (Scheme 2), which was subjected to an aromatic nucleophilic substitution with potassium phthalimide prepared *in situ* from **29** and K₂CO₃. Presumably due to the alkaline medium, the phthalimide ring was partially opened as detected by HPLC-MS. Upon attempted re-closing under reflux in AcOH, complete deprotection in fact took place and after purification aniline **30** was obtained with high purity. Compound **30** was used to introduce the iodine atom through a Sandmeyer reaction to give **28e** albeit in low yield. Reductive amination with **7** afforded amine **16e** followed by methylation to give *trans*-**6e** as an orange solid with 97% purity.

Table 3: Structure and results of photochemical and binding characterization of compounds 3e, 4d, 6b and 6d-i



3e, 4d, 6b, 6d-i

| Compound | Photochemistry | | | | | CXCR3 binding affinity | | | | |
|------------------------|------------------|---|---|--|-----|---|-----|---|-----|------------------|
| | Y | λ_{\max} <i>trans</i> π - π^* | λ_{\max} <i>cis</i> n - π^* | PSS ₃₆₀ (% area <i>cis</i>) ^b | SEM | pK _i <i>trans</i> ^c | SEM | pK _i PSS ₃₆₀ ^c | SEM | PAS ^d |
| 3e ^a | H | 323 | 421 | 88.9 | 0.4 | 6.3 | 0.0 | 5.6 | 0.0 | 5.0 |
| 6b ^a | F | 325 | 417 | 92.7 | 0.1 | 6.0 | 0.0 | 5.4 | 0.0 | 4.0 |
| 4d ^a | Cl | 328 | 422 | 92.6 | 0.2 | 5.9 | 0.0 | 5.6 | 0.0 | 2.0 |
| 6d ^a | Br | 333 | 420 | 92.6 | 0.2 | 5.8 | 0.0 | 5.4 | 0.0 | 2.5 |
| 6e | I | 339 | 424 | 90.5 | 1.0 | 5.5 | 0.1 | 5.5 | 0.0 | 1.0 |
| 6f ^a | OMe | 352 | 424 | 92.1 | 0.1 | 5.4 | 0.0 | 5.0 | 0.0 | 2.5 |
| 6g | O <i>i</i> Pr | 355 | 424 | 89.0 | 0.4 | 5.1 | 0.2 | 5.0 | 0.0 | 1.3 |
| 6h | SMe | 373 | ~425 ^e | 64.5 | 1.7 | 5.3 | 0.0 | 5.5 | 0.1 | 0.6 |
| 6i ^a | NMe ₂ | 387 | dec. ^f | dec. ^f | | | | | | |

^a Compound was previously described by us.⁷

^b % of *cis* isomer at the photostationary state (PSS₃₆₀) in PBS (25 μ M) measured after being pre-irradiated at 360 nm as obtained by LC/MS integration of the *cis* and *trans* isomer signals at 265 nm. The mean and SEM of at least two experiments are shown.

^c Binding affinity of *trans* isomer or PSS₃₆₀ as measured using [³H]-VUF11211 displacement. The mean and SEM of at least three experiments are shown.

^d The photoinduced affinity shift (PAS) was calculated as the ratio of the K_i *trans* and K_i PSS₃₆₀.

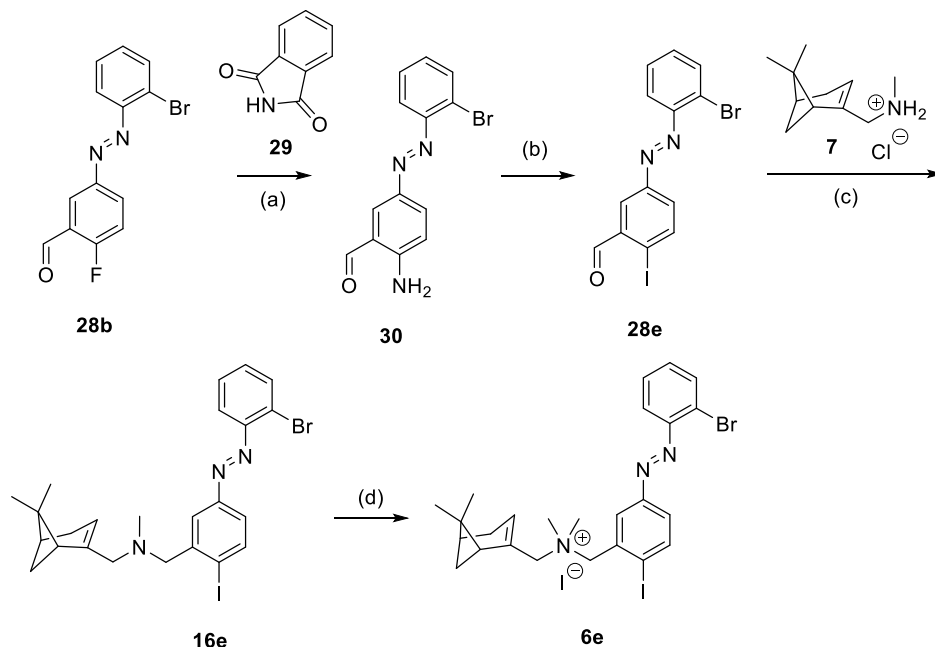
^e Could not be determined accurately due to partial overlapping of the π - π^* and n - π^* bands.

^f Compound decomposes under illumination.

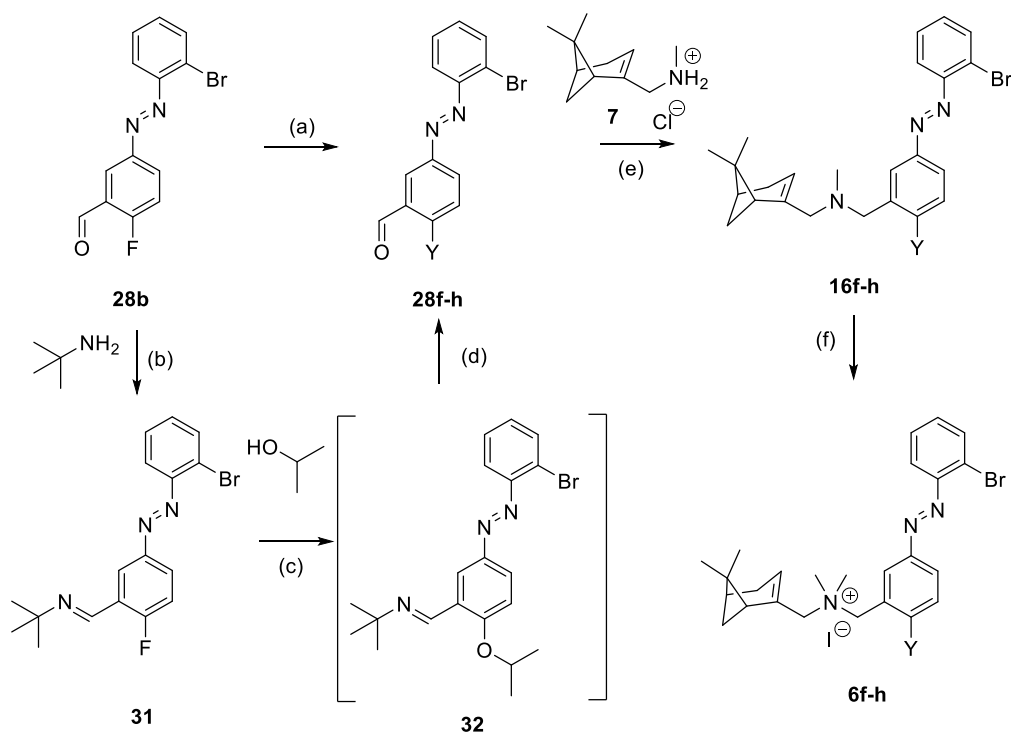
The synthesis of compounds **6f-h** was performed following a nucleophilic aromatic substitution route on **28b** (Scheme 4) since precursors **8** or **17** with the required substituent Y were not available. We performed nucleophilic aromatic substitutions with the corresponding sodium salts of MeOH, 2-PrOH and MeSH under MW irradiation. Both **28f** (Y=OMe) and **28h** (Y=SMe) were formed in high yields, but the conversion of the reaction with NaO*i*Pr was very low and partially gave reduction of the benzaldehyde. An alternative route utilized a method from Engle *et al* proceeding through a *tert*-butylimine intermediate (**32**) formed under Dean-Stark conditions.²³ This imine was reacted with NaO*i*Pr to form the ether **33**, which was subsequently hydrolyzed to obtain the desired aldehyde **28g** in high yield. Reductive amination of the aldehydes **28f-h** with **7** furnished amines **16f-h** which was followed by methylation to afford **6f-h** as orange solids with $\geq 98\%$ *trans* isomer. The synthetic strategies for the synthesis of compound **6i** were reported in our previous communication.⁷

In the subseries depicted in Table 3, several notable differences in both the UV-Vis spectra (Figure S1) and the photoisomerization rates were observed. When the substituent Y is a halogen atom, we observed a slight bathochromic shift of the π - π^* band to higher wavelengths with increasing size of the heteroatom, from 323 nm for Y = H (**3a**) to 339 nm for Y = I (**6e**) (Table 3, Figure 4A). When the group Y is OMe (**6f**), this shift is larger due to the higher EDG properties of MeO (λ_{\max} = 352 nm) and this is slightly further increased with Y=*i*OPr (**6g**, λ_{\max} = 355 nm). The shift is highest for Y=NMe₂ (**6i**, λ_{\max} = 380 nm). When the oxygen atom of **6f** was replaced by a sulphur atom, the bathochromic shift of the π - π^* band is also increased (**6h**, λ_{\max} = 373 nm, Table 3, Figure 4B). This high capacity of sulphur substituents to induce a bathochromic effect has already been reported in the azobenzene field.²⁴ The *trans-cis* photoisomerization for **6a-h** gave in general a high percentage of *cis* isomer (85-93%) with

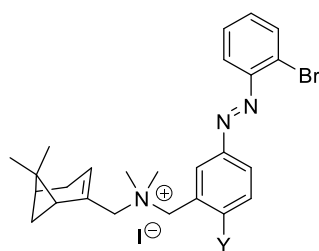
two exceptions. Compound **6h** shows a PSS of only 65% *cis* isomer due to a poor separation of the π - π^* and n - π^* bands as a result of the red-shifting prompted by the SMe group (Figure S1A,B), whereas **6i** decomposes upon irradiation with 360-nm light (as previously reported by us)⁷ leading to its exclusion from further characterization. The PSS₃₆₀ forms of exemplary compounds **4d**, **6e** and **6f** have thermal half-lives of 55, 28 and 29 days, respectively (10 μ M in HEPES buffer with 1% DMSO at 25 °C).



Scheme 3: Synthetic strategies for compounds 6e. Reagents and conditions: (a) i) K_2CO_3 (2.0 eq), DMF, MW, 65°C, 3 h; ii) AcOH, reflux, 1 h, 67%; (b) i) *p*TsOH·H₂O (3.0 eq), MeCN, 10-15 °C, 10 min; ii) NaNO₂ (2.0 eq), KI (2.5 eq), H₂O, 10-15 °C to rt, 2 h, 13%; (c) i) TEA (1.2 eq), DCM, rt, 10-30 min; ii) NaBH(OAc)₃ (1.6 eq), rt, 6-16 h, 54%; (f) MeI (20 eq), DCM, rt, 20 h, 57%.



Scheme 4: Synthetic strategies for compounds 6f-h. Reagents and conditions: (a) NaOMe or NaSMe (1.0-1.2 eq), MeOH or DMF, 65 °C, 30-60 min, 88-90%. (b) PhMe, 110 °C, Dean Stark, 20 h, 99%; (c) NaH (1.0 eq), DMSO, 100 °C, 1h; (d) THF/H₂O/AcOH 50:15:1, rt, 16 h, 79% (two steps); (e) i) TEA (1.3-1.4 eq), DCM, rt, 10-30 min; ii) NaBH(OAc)₃ (1.6 eq), rt, 6-16 h, 84-95%; (f) MeI (20 eq), DCM, rt, 20 h, 86-90%.

Table 4: Structure and results of functional characterization of compounds 3e, 4d, 6b and 6d-h**3e, 4d, 6b, 6d-h**

| Compound | Y | pEC ₅₀ ^{trans} ^b | | pEC ₅₀ ^{PSS₃₆₀} ^c | | α <i>trans</i> ^d | | α PSS ₃₆₀ ^e | | PDE ^f |
|------------------------|------|---|-------------------|---|-----|-----------------------------|-------------------|-----------------------------------|------|-------------------|
| | | SEM | SEM | SEM | SEM | SEM | SEM | SEM | SEM | |
| 1d | - | 6.9 | 0.0 | 6.9 | 0.0 | 1.04 | 0.08 | 1.03 | 0.07 | 0.00 |
| 3e ^a | H | n.m. ^g | n.m. ^g | 6.5 | 0.1 | 0.05 | 0.03 | 0.30 | 0.01 | 0.25 |
| 6b ^a | F | n.m. ^g | n.m. ^g | 6.2 | 0.1 | 0.12 | 0.00 | 0.41 | 0.03 | 0.30 |
| 4d ^a | Cl | n.m. ^g | n.m. ^g | 6.3 | 0.1 | 0.11 | 0.01 | 0.54 | 0.01 | 0.42 |
| 6d ^a | Br | n.m. ^g | n.m. ^g | 6.3 | 0.1 | 0.14 | 0.02 | 0.58 | 0.05 | 0.45 |
| 6e | I | 5.5 | 0.3 | 6.3 | 0.2 | 0.49 | 0.04 | 1.00 | 0.04 | 0.51 |
| 6f ^a | OMe | n.m. ^g | n.m. ^g | 6.4 | 0.1 | 0.16 | 0.01 | 0.99 | 0.04 | 0.83 |
| 6g | OiPr | n.m. ^h | n.m. ^h | 6.0 | 0.0 | n.m. ^h | n.m. ^h | 1.19 | 0.07 | n.m. ^h |
| 6h | SMe | 5.7 | 0.3 | 6.1 | 0.1 | 0.85 | 0.08 | 1.29 | 0.03 | 0.44 |

^a Compound was previously described by us.⁷

^b Potency of *trans* isomer in the dark. N.m.=not measurable. The mean and SEM of at least three experiments are shown.

^c Potency of a sample pre-irradiated at 360 nm to reach the photostationary state. The mean and SEM of at least three experiments are shown.

^d Intrinsic activity of *trans* isomer in the dark (CXCL11 efficacy set at α=1). The mean and SEM of at least three experiments are shown.

^e Intrinsic activity of a sample pre-irradiated at 360 nm to reach the photostationary state (CXCL11 efficacy set at α=1). The mean and SEM of at least three experiments are shown.

^f The photoinduced difference of efficacy (PDE) was obtained by subtracting α *trans* from α PSS₃₆₀.

^g Too low window.

^h The curve for *trans*-**6g** shows anomalous behavior at 10⁻⁵ M and higher.

The binding affinity of *trans*-**3e**, **4d**, **6b** and **6d-h** (Table 3) is in the low micromolar range with a low PAS value upon illumination. Initial pilot studies on [³⁵S]-GTPγS binding after CXCR3 stimulation with single concentrations of subseries **6** (data not shown) showed substantial levels of CXCR3 agonism in this group of compounds. For subseries **6** (and associated **3e** and **4d**) we therefore generated dose-response curves for the *trans* and PSS forms (Figure S2) using the same [³⁵S]-GTPγS functional assay and calculated the intrinsic activity (α) and potency (EC₅₀). As reported in our previous communication for some of the compounds,⁷ the PSS forms display agonism with high nanomolar potencies while most *trans* compounds are antagonists or partial agonists with very low efficacies (Table 4). However, when the size and/or EDG properties of Y increase, remarkably partial agonism with substantial efficacies appears even for the *trans* isomers, such as for **6e**, **6g** and **6h**. The compounds illuminated to PSS followed a similar qualitative trend: when the Y substituent H or F (**3e** and **5b**), the *cis* isomer behaves as a partial agonist with medium efficacy (α =0.27-0.41), but when the Y substituent increases in size and/or EDG properties, the efficacy increases to full efficacy with compounds **6e-h** (Y = I, OMe, OiPr and SMe). The *trans* form of **6g** shows anomalous behavior at 10⁻⁵ M and higher (Figure S2), preventing the extraction of accurate functional values. The PDE value, which reflects efficacies of both the *trans* and PSS form, appears to have an optimum for **6f** (Figure 4C). Figure 4C also shows more subtle versions of this for compounds **4d** and **6e**, which harbor a PDE value of 0.42 and 0.51, respectively, but in different parts of the efficacy window.

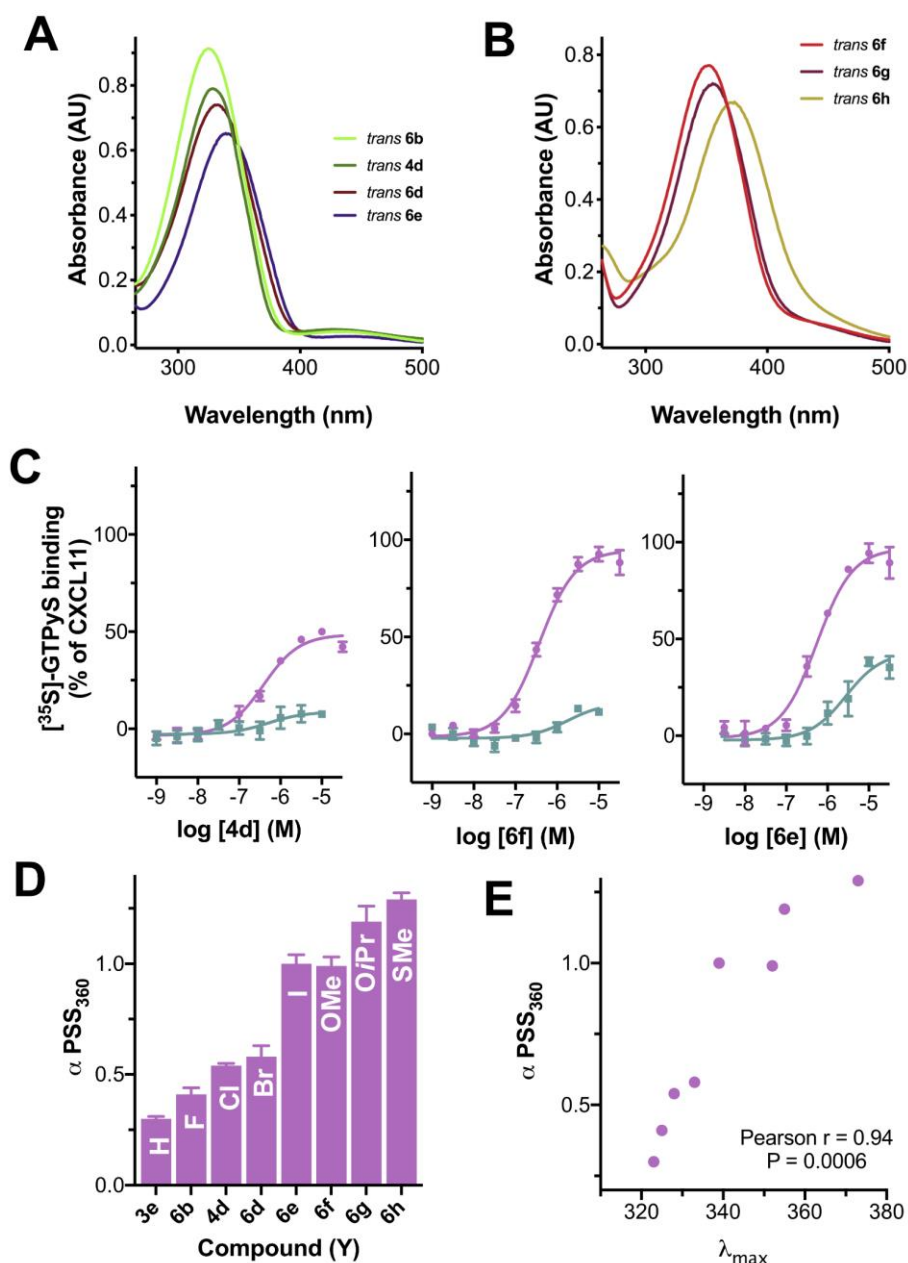


Figure 4: Properties of subseries 3e, 4d, 6b and 6d-h. (A,B) UV-Vis absorption spectra of *trans* isomers of (A) 6b, 4d, 6d and 6e (having substituent Y = F, Cl, Br and I respectively) or (B) 6f, 6g and 6h (having Y = OMe, OiPr and SMe respectively). (C) Functional dose-response curves using $[^3\text{S}]\text{-GTP}\gamma\text{S}$ assay exemplified for 4d, 6f and 6e, respectively (D) Summary of the efficacies of compounds 3e, 4d, 6b and 6d-h at PSS. (E) Correlation between the bathochromic shifting of the π - π^* band and the intrinsic activity of PSS forms for the compounds in Table 4.

The results reveal that the electron density of the aryl rings, especially of the inner one, plays a key role in inducing agonism in CXCR3. In general, the *cis* isomers of the series 2-6 are better CXCR3 agonists. Indeed, the *cis* isomers generally are assumed to have intrinsically higher electron density due to the disruption of the conjugation between the two rings of the azobenzene through the N=N bond. Moreover, the electronic properties of the inner substituent Y have been proven to be of strategic use in increasing the intrinsic activity (α) of the *cis* form of the ligands (Figure 4D). This capacity of the Y substituent to alter the electron density is conceivably related to its capacity to induce a bathochromic shift of the π - π^* band of the *trans* isomer. In fact, the bathochromic shift and intrinsic

activity of the *cis* isomers (PSS₃₆₀) properties are correlated well (Figure 4E, Pearson $r = 0.94$, $P = 0.0006$) for the subseries of compounds **3e**, **4d**, **6b** and **6d-h**.

Conclusions

We designed and synthesized a toolbox of 31 photochromic small-molecule CXCR3 receptor ligands based on the azologization of a biaryl series reported previously by us. All compounds show affinity for CXCR3 from the high nanomolar to the low micromolar range. Our efforts, however, were focused on exploring the landscape in functional efficacy. To this end, the scaffold was subjected to positional and substitution changes in structure, necessitating extensive synthetic efforts through multiple routes. The presence of halogen substituents on the *ortho* position of the outer ring (substituent X) provides partial agonism for the *cis* isomer with a Br atom being the major exponent, while *trans* isomers preserve antagonist behavior. The presence of a substituent on the *para* position of the central ring (substituent Y) capable of delocalizing π electrons increases the efficacy of the *cis* isomer. *Cis* isomers of compounds with Y = I, OMe, *OiPr* or SMe are all full agonists of CXCR3, however the corresponding *trans* isomers also activate the receptor to varying degrees. In all, our efforts deliver a spectrum of (subtle) efficacy differences. Notable tool compounds are VUF15888 (**4d**) switching from antagonism to partial agonism (PDE = 0.42), VUF16620 (**6e**) switching from partial agonism to full agonism (PDE = 0.60), and VUF16216 (**6f**), which represents the optimum balance and provides a CXCR3 photoswitch with a PDE value of 0.83, i.e. from antagonism to full agonism. These compounds will be valuable tools for future photopharmacological studies on the dynamic signaling of the chemokine receptor CXCR3.

Acknowledgments

All authors acknowledge the Netherlands Organization for Scientific Research for financial support (TOPPUNT, “7 ways to 7TMR modulation (7-to-7)”, 718.014.002). We thank Danny Scholten, Chris de Graaf, and Luc Roumen for helpful discussions, Hans Custers for recording HRMS spectra and Mounir Andaloussi for providing key building block **7**.

References

- (1) Hüll, K.; Morstein, J.; Trauner, D. *Chem. Rev.* **2018**, *118* (21), 10710–10747.
- (2) Hoorens, M. W. H.; Szymanski, W. *Trends Biochem. Sci.* **2018**, *43* (8), 567–575.
- (3) Hauwert, N. J.; Mocking, T. A. M.; Da Costa Pereira, D.; Kooistra, A. J.; Wijnen, L. M.; Vreeker, G.; Verweij, N. W. E.; De Boer, B. H.; Smit, M. J.; de Graaf, C.; et al. *J. Am. Chem. Soc.* **2018**, *140* (12), 4232–4243.
- (4) Donthamsetti, P. C.; Winter, N.; Schönberger, M.; Levitz, J.; Stanley, C.; Javitch, J. A.; Isacoff, E. Y.; Trauner, D. *J. Am. Chem. Soc.* **2017**, *139* (51), 18522–18535.
- (5) Lachmann, D.; Konieczny, A.; Keller, M.; König, B. *Org. Biomol. Chem.* **2019**, *17* (9), 2467–2478.
- (6) Westphal, M. V.; Schafroth, M. A.; Sarott, R. C.; Imhof, M. A.; Bold, C. P.; Leippe, P.; Dhopeswarkar, A.; Grandner, J. M.; Katritch, V.; Mackie, K.; et al. *J. Am. Chem. Soc.* **2017**, *139* (50), 18206–18212.

- (7) Gómez-Santacana, X.; de Munnik, S. M.; Vijayachandran, P.; Da Costa Pereira, D.; Bebelman, J. P. M.; de Esch, I. J. P.; Vischer, H. F.; Wijtmans, M.; Leurs, R. *Angew. Chemie - Int. Ed.* **2018**, *57* (36), 11608–11612.
- (8) Morstein, J.; Awale, M.; Reymond, J.-L.; Trauner, D. *ACS Cent. Sci.* **2019**, *5* (4), 607–618.
- (9) Hartley, G. S. *Nature* **1937**, *140* (3537), 281.
- (10) Ricart-Ortega, M.; Font, J.; Llebaria, A. *Mol. Cell. Endocrinol.* **2019**, *488*, 36–51.
- (11) Hauwert, N. J.; Mocking, T. A. M.; Da Costa Pereira, D.; Lion, K.; Huppelschoten, Y.; Vischer, H. F.; De Esch, I. J. P.; Wijtmans, M.; Leurs, R. *Angew. Chemie - Int. Ed.* **2019**, *58*, 4531–4535.
- (12) Hauser, A. S.; Attwood, M. M.; Rask-Andersen, M.; Schioth, H. B.; Gloriam, D. E. *Nat. Rev. Drug Discov.* **2017**, *16* (12), 829–842.
- (13) Schönberger, M.; Trauner, D. *Angew. Chemie - Int. Ed.* **2014**, *53* (12), 3264–3267.
- (14) Pittolo, S.; Gómez-Santacana, X.; Eckelt, K.; Rovira, X.; Dalton, J.; Goudet, C.; Pin, J.-P.; Llobet, A.; Giraldo, J.; Llebaria, A.; et al. *Nat. Chem. Biol.* **2014**, *10* (10), 813–815.
- (15) Bahamonde, M. I.; Taura, J.; Paoletta, S.; Gakh, A. A.; Chakraborty, S.; Hernando, J.; Fernández-Dueñas, V.; Jacobson, K. A.; Gorostiza, P.; Ciruela, F. *Bioconjug. Chem.* **2014**, *25* (10), 1847–1854.
- (16) Gomez-Santacana, X.; Pittolo, S.; Rovira, X.; Lopez, M.; Zussy, C.; Dalton, J. A.; Faucherre, A.; Jopling, C.; Pin, J. P.; Ciruela, F.; et al. *ACS Cent. Sci.* **2017**, *3* (1), 81–91.
- (17) Wijtmans, M.; Scholten, D. J.; Roumen, L.; Canals, M.; Custers, H.; Glas, M.; Vreeker, M. C.; de Kanter, F. J.; de Graaf, C.; Smit, M. J.; et al. *J. Med. Chem.* **2012**, *55* (23), 10572–10583.
- (18) Wijtmans, M.; Scholten, D.; Mooij, W.; Smit, M. J.; de Esch, I. J. P.; de Graaf, C.; Leurs, R. Exploring the CXCR3 Chemokine Receptor with Small-Molecule Antagonists and Agonists. In *Chemokines: Chemokines and Their Receptors in Drug Discovery*; Tschammer, N., Ed.; Springer International Publishing: Cham, 2015; pp 119–185.
- (19) MOE, Version 2016.0802; Chemical Computing Group, Inc.; Montreal, Canada.
- (20) Fliegl, H.; Köhn, A.; Hättig, C.; Ahlrichs, R. *J. Am. Chem. Soc.* **2003**, *125* (32), 9821–9827.
- (21) Wijtmans, M.; Verzijl, D.; Bergmans, S.; Lai, M.; Bosch, L.; Smit, M. J.; de Esch, I. J.; Leurs, R. *Bioorg. Med. Chem.* **2011**, *19* (11), 3384–3393.
- (22) Scholten, D. J.; Wijtmans, M.; van Senten, J. R.; Custers, H.; Stunnenberg, A.; de Esch, I. J.; Smit, M. J.; Leurs, R. *Mol. Pharmacol.* **2015**, *87* (4), 639–648.
- (23) Engle, K. M.; Luo, S. X.; Grubbs, R. H. *J. Org. Chem.* **2015**, *80* (8), 4213–4220.
- (24) Nishioka, H.; Liang, X.; Kato, T.; Asanuma, H. *Angew. Chemie Int. Ed.* **2012**, *51* (5), 1165–1168.